

**Fabrication of Thin Film, Flexible and Transparent Electrodes Composed of Ruthenic Acid Nanosheets by Electrophoretic Deposition and Application to Electrochemical Capacitors**

Wataru Sugimoto,<sup>\*,z</sup> Katsunori Yokoshima, Kazunori Ohuchi, Yasushi Murakami, and Yoshio Takasu<sup>\*</sup>

Department of Fine Materials Engineering, Faculty of Textile Science and Technology, Shinshu University, 3-15-1 Tokida, Ueda 386-8567, JAPAN

\* Electrochemical Society Active Member

<sup>z</sup> E-mail: wsugi@shinshu-u.ac.jp

FAX: +81-268-21-5452

Keywords: Electrochemical capacitors, Electrophoretic deposition, Transparent, flexible electrodes

## ABSTRACT

Ruthenic acid nanosheet colloids were prepared by dispersing a tetrabutylammonium-ruthenic acid intercalation compound in acetonitrile, or *N,N*-dimethylformamide. Nanosheet electrodes were fabricated on gold, indium-tin oxide (ITO)-coated glass, and ITO-coated PET electrodes by electrophoretic deposition using these colloids. Transparent or flexible electrodes could be fabricated by using ITO electrodes as the substrate. The deposited amount of material could easily be controlled by the extent of deposition, which was confirmed from the linear increase in specific capacitance as a function of the deposition time. The ruthenic acid nanosheet electrodes using Au substrates exhibited gravimetric capacitance of  $620 \text{ F (g-RuO}_2\text{)}^{-1}$ . Specific capacitance of  $0.82 \text{ F cm}^{-2}_{(\text{geometric})}$  was achieved at a scan rate of  $2 \text{ mV s}^{-1}$  with a film deposited at  $5 \text{ V cm}^{-1}$  for 1 h.

## Introduction

Electrochemical capacitors (also known as supercapacitors or ultracapacitors) that utilize ruthenium-based oxides as electrode material can provide a combination of high power density, high energy density and long cycle life owing to their good electronic conductivity, proton conductivity, electrochemical stability, and redox behavior.<sup>1-8</sup> Thus, such devices may find application in power sources such as hybrid vehicles, portable electronic devices, and short term back-up. In particular, nanostructured-ruthenium oxides possessing structural water –for example nanoparticulate ruthenium oxide hydrate ( $\text{RuO}_2 \cdot n\text{H}_2\text{O}$ )<sup>9,10</sup> and layered ruthenic acid hydrate ( $\text{H}_{0.2}\text{RuO}_{2.1} \cdot x\text{H}_2\text{O}$ )<sup>11-13</sup> – can provide high energy density due to the high electrochemically active surface area. A difficulty in the use of such hydrous oxides as electrode materials is that the use of typical hot-press and post-annealing methods for electrode fabrication, which is essential for decreasing the charge transfer resistance and mechanical stability, cannot be applied. Typical sheet- or coin-type electrode fabrication procedures involve the physical mixing of the active material, conducting carbon additives, and binders such as PTFE.<sup>1</sup> Heat treatment is often conducted at temperatures near the melting point of the binder (320°C) to ensure good contact. At such high temperatures, irreversible loss of water, structural transformation, and particle growth seriously reduce the charge storage capability. Thus low temperature coating techniques must be applied.

Layered ruthenates are characterized by excellent electronic and protonic conductivity as well as electrochemical stability in aqueous electrolytes, making them excellent candidates as electrode material for electrochemical capacitors.<sup>11-14</sup> We recently developed a stable colloid consisting of ruthenic acid nanosheets (HROns)

derived from a layered potassium ruthenate. These nanosheets are composed of negatively charged oxide sheets with lateral dimension in the order of micrometers and thickness less than 1 nm. A thin film electrode composed of re-stacked HROns modified glassy carbon electrode prepared by a simple casting method exhibited specific capacitance up to  $660 \text{ F g}^{-1}$ .<sup>11</sup> However, the modification of the glassy carbon electrode with re-stacked HROns was limited to about  $20 \mu\text{g-RuO}_2 \text{ cm}^{-2}$ . This is most likely due to the weak interaction between the substrate and re-stacked HROns, leading to mechanical instability for thicker films.

Transition-metal oxide nanosheets have attracted increased interest in electrochemical applications for energy conversion and storage due to its low dimensionality, high surface area, and photo/electro-functionality.<sup>11,15-23</sup> The nanosheets can be used as building blocks owing to their colloidal nature as polyelectrolytes with intrinsic negative charge. By utilizing the intrinsic negative charge of the nanosheets, thin film electrodes have been fabricated via electrostatic layer-by-layer deposition<sup>20,24-31</sup> or electrophoretic deposition (EPD).<sup>15-17,32,33</sup> The EPD method is a distinguished technique for obtaining uniform films with varying thickness, and is based on the electrophoresis of charged colloidal particles under the influence of an electric field.<sup>34,35</sup> Thus, the EPD method depends on colloidal science and does not rely on conventional powder technology. Advantages of the EPD technique include good adhesion properties with the substrate, room-temperature fabrication, large-scale fabrication, and binder free fabrication. Another advantage is that in the case of EPD of nanosheets, the inorganic nanosheets can be isolated from the organic cations.<sup>32</sup>

Here, we report the electrophoretic deposition of negatively-charged HROns onto

gold or ITO-coated substrates using a nanosheet colloid. The utilizing of the EPD method for nanosheet electrode fabrication has allowed us to overcome the difficulties associated with electrode fabrication of hydrous oxides in terms of adhesion to the substrate, control of amount deposited, and utilization of ruthenium.

### Experimental Section

The ruthenic acid nanosheet colloid was prepared following a similar procedure to an earlier report.<sup>11</sup> Briefly, layered potassium ruthenate ( $\text{K}_{0.2}\text{RuO}_{2.1}\cdot x\text{H}_2\text{O}$ ) was prepared by solid-state reaction of  $\text{K}_2\text{CO}_3$  and  $\text{RuO}_2$  (5:8 molar ratio) at  $850^\circ\text{C}$  for 12 h under Ar flow. Layered potassium ruthenate was converted to layered ruthenic acid hydrate ( $\text{H}_{0.2}\text{RuO}_{2.1}\cdot x\text{H}_2\text{O}$ ) by acid treatment at  $60^\circ\text{C}$  for 48 h followed by washing with copious amounts of water and drying at  $120^\circ\text{C}$ . An ethylammonium-ruthenic acid intercalation compound was prepared by reaction of  $\text{H}_{0.2}\text{RuO}_{2.1}\cdot x\text{H}_2\text{O}$  with a 50% ethylamine aqueous solution at room temperature for 24 h. A tetrabutylammonium-layered ruthenic acid intercalation compound was prepared by reaction of the ethylammonium-ruthenic acid intercalation compound with a 10% tetrabutylammonium hydroxide aqueous solution at room temperature for 50 h. The solid product was centrifugally collected (15,000 rpm). The stability of the nanosheet colloid in various high permittivity solvents was studied by dispersing the tetrabutylammonium-ruthenic acid intercalation compound in methanol, ethanol, acetonitrile (AN), or *N,N*-dimethylformamide (DMF). The suspension was subject to ultrasonification for 30 min and centrifuged at 2,000 rpm. The supernatant was used for further investigation.

Electrophoretic deposition (EPD) was conducted in a similar method to the deposition of titanate acid nanosheets.<sup>32</sup> A Pt mesh (2.25 cm<sup>2</sup>) and a Au plate (1 cm<sup>2</sup>) was used as the cathode and anode, respectively. For the transparent and flexible electrodes, indium-tin oxide (ITO)-coated glass electrodes (Nippon Sheet Glass Co.; thickness 1.1 mm (200 nm ITO); 7-13 Ω/sq, 2.25 cm<sup>2</sup> active area) and ITO-coated PET electrodes (Tobi Co.; OTEC; 113B-N125N; thickness 125 μm; 10-20 Ω/sq, 2.25 cm<sup>2</sup> active area) were used as the anode. The electrodes were placed parallel with a distance of  $d_{\text{EPD}}=10$  mm into the HROs colloid, and a constant potential,  $E_{\text{EPD}}$ , of 5 V was applied for  $t_{\text{EPD}}=2-60$  min at room temperature unless otherwise noted. The as-deposited films were dried under ambient conditions.

The structure of the products was studied by X-ray diffraction (XRD) (Rigaku RINT 2550H/PC; monochromated Cu K $\alpha$  radiation). Field-emission scanning-electron microscopy (FE-SEM) (Hitachi S-5000) was utilized for morphological observation of the products. UV-Vis spectra were recorded on a Shimadzu UV-Visible spectrophotometer UV-2400. A beaker-type electrochemical cell was used for the electrochemical measurements of the EPD films using Au as the substrate. The cell was equipped with the EPD film as the working electrode, a platinum mesh counter electrode, and an Ag/AgCl reference electrode. A Luggin capillary faced the working electrode at a distance of 2 mm. Electrode potentials will be referred to the reversible hydrogen electrode (RHE) potential scale. Cyclic voltammetry was carried out between 0.2 and 1.2 V vs. RHE at scan rates of 2-200 mV s<sup>-1</sup> at 25°C in 0.5 M H<sub>2</sub>SO<sub>4</sub>. The capacitance was calculated by averaging the anodic and cathodic charge after at least 500 break-in cycles. Electrochemical measurements of the ITO-coated electrodes were

studied in a two-electrode configuration composed of two HRONs/ITO-coated glass electrodes sandwiched between a Nafion 117 membrane and immersed in 0.5 M H<sub>2</sub>SO<sub>4</sub>.

## Results and Discussion

*Stability of nanosheet colloids during the EPD process in various solvents.*— One of the necessities for EPD is that the colloid is well dispersed and stable. The careful choice of solvent is often a key to success in EPD. Dispersion of the tetrabutylammonium-ruthenic acid intercalation compound in acetonitrile (AN) and *N,N*-dimethylformamide (DMF) resulted in stable HRONs colloids (Fig. 1). EPD using these colloids was visually recognized at the anode. No sedimentation was observed during the EPD process. The XRD patterns of the HRONs/Au films with  $t_{\text{EPD}}=10$  min using HRONs colloids in AN and DMF (hereafter denoted HRONs(AN)/Au and HRONs(DMF)/Au) are shown in Fig. 2. The interlayer distance of the deposited material was dependent on the solvent,  $d=0.95$  and  $0.82$  nm for HRONs(AN)/Au and HRONs(DMF)/Au, respectively. These values are smaller than the tetrabutylammonium-ruthenic acid intercalation compound ( $d=1.69$  nm), indicating the anodic deposition of the negatively charged nanosheets onto the Au substrate. The fact that the interlayer distance is smaller than the precursor tetrabutylammonium-ruthenic acid intercalation compound strongly suggests that the amount of TBA in the deposited film is insignificant. The interlayer distance of the HRONs/Au EPD films are larger than pristine ruthenic acid ( $d=0.46$  nm), suggesting solvent co-intercalation into the interlayer during the EPD process. Typical surface SEM images of HRONs(AN)/Au and HRONs(DMF)/Au ( $t_{\text{EPD}}=10$  min) are shown in Fig. 3. The images reveal flexible

HROns covering the substrate uniformly.

A stable HROns colloid could also be obtained by dispersion of the tetrabutylammonium-ruthenic acid intercalation compound in methanol (Fig. 1c). However, when the HROns colloid in methanol was used for EPD, deposition was barely visible and sedimentation was observed during the EPD process. XRD analysis of the precipitate revealed a low-angle XRD peak at  $d=0.8$  nm, which is different from that of the tetrabutylammonium-ruthenic acid intercalation compound or pristine layered ruthenic acid. These observations indicate a reaction between the HROns and methanol occurred during the EPD process. In order to understand the instability of the colloid when using methanol as the solvent, the tetrabutylammonium-ruthenic acid intercalation compound was dispersed in ethanol. In this case, a precipitate was obtained (Fig. 1d). The XRD pattern of the precipitate after drying at room temperature showed a low-angle XRD peak at  $d=1.29$  nm. The interlayer distance was unchanged even after drying the product at 120°C, thus the intercalation of ethanol molecules into the interlayer is unlikely. It is suggested that the surface hydroxy groups of ruthenic acid reacted with ROH (R=CH<sub>3</sub> and C<sub>2</sub>H<sub>5</sub>) to yield an alcoxy-modified ruthenium oxide (Ru-OH + HOR → Ru-OR + H<sub>2</sub>O). Similar interlayer hydroxy modification reactions have been reported for several layered compounds.<sup>36-47</sup>

*Electrochemical characterization of HROns/Au.*— Steady-state cyclic voltammograms (CVs) at 2 mV s<sup>-1</sup> of HROns(AN)/Au and HROns(DMF)/Au films ( $t_{\text{EPD}}=10$  min) are compared in Fig. 4. The CV profile is similar to that of the re-stacked HROns modified glassy carbon electrode. The specific capacitance was 360 and 150 mF

$\text{cm}^{-2}$  for HROns(AN)/Au and HROns(DMF)/Au, respectively. The larger specific capacitance of HROns(AN)/Au is most likely due to a larger amount of HROns deposit, owing to the lower viscosity of AN (AN: 0.325 mPa s, DMF: 0.802 mPa s). The capacitance values are considerably larger than the re-stacked HROns modified glassy carbon electrode prepared by a casting method ( $12 \text{ mF cm}^{-2}_{(\text{geometric})}$ ) with  $20 \mu\text{g-RuO}_2 \text{ cm}^{-2}$ . Assuming that all of the HROns in the HROns(AN)/Au electrode ( $t_{\text{EPD}}=10 \text{ min}$ ) is electrochemically active, the deposited mass can be estimated as  $550 \mu\text{g-RuO}_2 \text{ cm}^{-2}$ . Hence it is obvious that a significant increase in deposited mass was achieved by EPD.

For comparison, EPD ( $t_{\text{EPD}}=30 \text{ min}$ ) was conducted with pristine (non-exfoliated) HRO and hydrous ruthenium oxide ( $\text{RuO}_2 \cdot 0.5\text{H}_2\text{O}$ ) dispersed in DMF. Although a small amount of HRO was deposited on the anode, the specific capacitance was significantly low ( $<2 \text{ mF cm}^{-2}$ ). When  $\text{RuO}_2 \cdot 0.5\text{H}_2\text{O}$  was used, no deposition was confirmed at the anode or cathode. It is clear that under the present experimental conditions, the use of HROns colloid is essential for the EPD process.

Cyclic voltammograms at a scan rate of  $2 \text{ mV s}^{-1}$  of HROns(DMF)/Au prepared with  $t_{\text{EPD}}=2-60 \text{ min}$  are shown in Fig. 5. The specific capacitances of each electrode at various scan rates are plotted in Fig. 6. A constant increase in capacitance was obtained with an increase in  $t_{\text{EPD}}$  at a scan rate of  $2 \text{ mV s}^{-1}$ , with a rate of  $13.6 \text{ mF cm}^{-2} \text{ min}^{-1}$ . A slight deviation from linearity is observed with increasing  $t_{\text{EPD}}$  at higher scan rates. This is attributed to an increase in resistance because of the increase in film thickness. The capacitance can be divided into the non-Faradaic electrical-double layer capacitance and Faradaic surface-redox charge.<sup>11,12</sup> The fact that both the electric double layer capacitance and surface redox charge increase linearly with  $t_{\text{EPD}}$  (thus the deposited

amount of HRONS) indicates that the interlayer region is active for charge storage. The stability of the HRONS(DMF)/Au ( $t_{\text{EPD}}=10$  min) is demonstrated in Fig. 7 upon cycling at  $50 \text{ mV s}^{-1}$  for 10,000 cycles. Although a slight decrease in the redox peak current at  $\sim 0.65 \text{ V vs. RHE}$  is observed, the CV profile is quite stable. Note that the electric double layer capacitance is unchanged after 10,000 cycles, indicating the high electrochemical and mechanical stability of the EPD film.

The HRONS(DMF)/Au film obtained with  $t_{\text{EPD}}=30$  min was annealed at  $600^\circ\text{C}$  in air for 3 h to convert HRONS to  $\text{RuO}_2$ . The mass increase relative to the Au substrate was determined to be  $0.64 \text{ mg-RuO}_2$ . Thus the gravimetric capacitance is  $620 \text{ F (g-RuO}_2)^{-1}$  for this electrode, which is comparable with that of ruthenic-acid nanosheet modified glassy carbon electrode,  $660 \text{ F (g-RuO}_2)^{-1}$ . Combined with the linear increase in specific capacitance as a function of  $t_{\text{EPD}}$ , it is obvious that all of the deposited HRONS are electrochemically active for charge storage.

*Electrochemical characterization of HRONS/ITO.*— Figure 8 shows photographs of EPD films using tetrabutylammonium-ruthenic acid intercalation compound in DMF and ITO-coated glass or ITO-coated PET substrates as the anode. Transparent or flexible HRONS films were obtained. The HRONS films have fairly good transmittance in the visible region (Fig. 9). Figure 8c shows a typical side-view FE-SEM image of HRONS/ITO-coated glass electrode prepared with  $t_{\text{EPD}} = 2 \text{ min} \times 15$  times. It can be seen that the flexible nanosheets pile up parallel to the substrate. The thickness of the ruthenic acid nanosheet film for this particular (non-transparent) electrode was about 500 nm. Figure 10 shows CVs of a cell composed of two HRONS/ITO-coated glass

electrodes sandwiched between a Nafion 117 membrane and immersed in 0.5 M H<sub>2</sub>SO<sub>4</sub>. Specific capacitance of c.a. 3 mF cm<sup>-2</sup> was achieved with this device at a scan rate of 2 mV s<sup>-1</sup>. The specific capacitance increases linearly with increasing  $t_{EPD}$  (Fig. 10b), though high capacitance electrodes are less transparent. Constant current charge/discharge studies (Fig. 11) shows that the device exhibits capacitive behavior. Figure 12 shows the cyclability of the device up to 1,000 cycles. A slight decrease in capacitance is observed, which is attributed to the instability of ITO.

### Conclusion

We have demonstrated that electrophoretic deposition of ruthenic acid nanosheets using stable nanosheet colloids is an effective method to fabricate electrodes with high energy density at room temperature. Varying the duration of EPD could easily control the deposited amount of material. It has been confirmed that all of the deposited material is electrochemically active for charge storage. The ruthenic acid nanosheet electrodes can deliver mass specific capacitance of 620 F (g-RuO<sub>2</sub>)<sup>-1</sup>. Specific capacitance of 0.82 F cm<sup>-2</sup><sub>(geometric)</sub> was achieved at a scan rate of 2 mV s<sup>-1</sup> with a film deposited at 5 V cm<sup>-1</sup> for 1 h. Furthermore, transparent, flexible electrodes could be prepared by using ITO-coated electrodes instead of a Au plate.

**Acknowledgements.** This work was supported in part by an Industrial Technology

Research Grant Program from the New Energy and Industrial Technology Development Organization (NEDO), a Grant-in-Aid for Scientific Research No.16750170 and a 21st Century COE Program from MEXT. W.S. would like to thank the Asahi Glass Foundation for financial support.

## References

1. B.E. Conway, *Electrochemical Supercapacitors*, Kluwer Academic Pub., Norwell, MA (1999).
2. A. Burke, *J. Power Sources*, **91**, 37 (2000).
3. B.E. Conway, *J. Electrochem. Soc.*, **138**, 1539 (1991).
4. S. Trasatti, *Electrochim. Acta*, **36**, 225 (1991).
5. S. Sarangapani, B.V. Tilak, C.-P. Chen, *J. Electrochem. Soc.*, **143**, 3791 (1996).
6. B.E. Conway, V. Birss, J. Wojtowicz, *J. Power Sources*, **66**, 1 (1997).
7. Y. Takasu, Y. Murakami, *Electrochim. Acta*, **45**, 4135 (2000).
8. C. Angelinetta, S. Trasatti, L.D. Atanasoska, R.T. Atanasoski, *J. Electroanal. Chem.*, **214**, 535 (1986).
9. J.P. Zheng, T.R. Jow, *J. Electrochem. Soc.*, **142**, L6 (1995).
10. J.P. Zheng, P.J. Cyang, T.R. Jow, *J. Electrochem. Soc.*, **142**, 2699 (1995).
11. W. Sugimoto, H. Iwata, Y. Yasunaga, Y. Murakami, Y. Takasu, *Angew. Chem. Int. Ed.*, **42**, 4092 (2003).

12. W. Sugimoto, H. Iwata, Y. Murakami, Y. Takasu, *J. Electrochem. Soc.*, **151**, A1181 (2004).
13. W. Sugimoto, H. Iwata, K. Yokoshima, Y. Murakami, Y. Takasu, *J. Phys. Chem. B*, **109**, 7330 (2005).
14. W. Sugimoto, M. Omoto, K. Yokoshima, Y. Murakami, Y. Takasu, *J. Solid State Chem.*, **177**, 4542 (2004).
15. Y. Matsumoto, A. Funatsu, D. Matsuo, U. Unal, K. Ozawa, *J. Phys. Chem. B*, **105**, 10893 (2001).
16. M. Koinuma, H. Seki, Y. Matsumoto, *J. Electroanal. Chem.*, **531**, 81 (2002).
17. U. Unal, Y. Matsumoto, N. Tanaka, Y. Kimura, N. Tamoto, *J. Phys. Chem. B*, **107**, 12680 (2003).
18. L. Wang, K. Takada, A. Kajiyama, M. Onoda, Y. Michiue, L. Zhang, M. Watanabe, T. Sasaki, *Chem. Mater.*, **15**, 4508 (2003).
19. Y. Omomo, T. Sasaki, L. Wang, M. Watanabe, *J. Am. Chem. Soc.*, **125**, 3568 (2003).
20. F. Huguenin, M. Ferreira, V. Zucolotto, F.C. Nart, R.M. Torresi, O.N. Oliveira, Jr.,

- Chem. Mater.*, **16**, 2293 (2004).
21. N. Sakai, Y. Ebina, K. Takada, T. Sasaki, *J. Am. Chem. Soc.*, **126**, 5851 (2004).
  22. J. He, P. Yang, H. Sato, Y. Umemura, A. Yamagishi, *J. Electroanal. Chem.*, **566**, 227 (2004).
  23. L. Wang, N. Sakai, Y. Ebina, K. Takada, T. Sasaki, *Chem. Mater.*, **17**, 1352 (2005).
  24. T. Sasaki, Y. Ebina, T. Tanaka, M. Harada, M. Watanabe, *Chem. Mater.*, **13**, 4661 (2001).
  25. T. Sasaki, Y. Ebina, K. Fukuda, T. Tanaka, M. Harada, M. Watanabe, *Chem. Mater.*, **14**, 3524 (2002).
  26. L. Wang, Y. Omomo, N. Sakai, K. Fukuda, I. Nakai, Y. Ebina, K. Takada, M. Watanabe, T. Sasaki, *Chem. Mater.*, **15**, 2873 (2003).
  27. Z.-S. Wang, T. Sasaki, M. Muramatsu, Y. Ebina, T. Tanaka, L. Wang, M. Watanabe, *Chem. Mater.*, **15**, 807 (2003).
  28. L. Wang, Y. Ebina, K. Takada, T. Sasaki, *Chem. Commun.*, 1074 (2004).
  29. T. Tanaka, K. Fukuda, Y. Ebina, K. Takada, T. Sasaki, *Ad. Mater.*, **16**, 872 (2004).
  30. R. Ma, T. Sasaki, Y. Bando, *J. Am. Chem. Soc.*, **126**, 10382 (2004).

31. L. Wang, Y. Ebina, K. Takada, T. Sasaki, *J. Phys. Chem. B*, **108**, 4283 (2004).
32. W. Sugimoto, O. Terabayashi, Y. Murakami, Y. Takasu, *J. Mater. Chem.*, **12**, 3814 (2002).
33. T. Yui, Y. Mori, T. Tsuchino, T. Itoh, T. Hattori, Y. Fukushima, K. Takagi, *Chem. Mater.*, **17**, 206 (2005).
34. P. Sarkar, P. S. Nicholson, *J. Am. Ceram. Soc.*, **79**, 1987 (1996).
35. M. S. J. Gani, *Indust. Ceram.*, **14**, 163 (1994).
36. S. Takahashi, T. Nakato, S. Hayashi, Y. Sugahara, K. Kuroda, *Inorg. Chem.*, **34**, 5065 (1995).
37. H. Suzuki, K. Notsu, Y. Takeda, W. Sugimoto, Y. Sugahara, *Chem. Mater.*, **15**, 636 (2003).
38. S. Tahara, Y. Sugahara, *Langmuir*, **19**, 9473 (2003).
39. S. Yoshioka, Y. Takeda, Y. Uchimaru, Y. Sugahara, *J. Organomet. Chem.*, **686**, 145 (2003).
40. Y. Mitamura, Y. Komori, S. Hayashi, Y. Sugahara, K. Kuroda, *Chem. Mater.*, **13**, 3747 (2001).

41. J.J. Tunney, C. Detellier, *Chem. Mater.*, **5**, 747 (1993).
42. Y. Komori, H. Enoto, R. Takenawa, S. Hayashi, Y. Sugahara, K. Kuroda,  
*Langmuir*, **16**, 5506 (2000).
43. S. Kikkawa, F. Kanamaru, M. Koizumi, *Inorg. Chem.*, **15**, 2195 (1976).
44. S. Yamanaka, *Inorg. Chem.*, **15**, 2811 (1976).
45. J.W. Johnson, A.J. Jacobson, W.M. Butler, S.E. Rosenthal, J.F. Brody, J.T.  
Lewandowski, *J. Am. Chem. Soc.*, **111**, 381 (1989).
46. M. Ogawa, S. Okutomo, K. Kuroda, *J. Am. Chem. Soc.*, **120**, 7361 (1998).
47. S. Tahara, Y. Sugahara, *Recent Res. Develop. Inorg. Chem.*, **4**, 13 (2004).

## Figure Captions

Figure 1. Photographs of tetrabutylammonium-ruthenic acid intercalation compound dispersed in a) acetonitrile, b) *N,N*-dimethylformamide, c) methanol, and d) ethanol.

Figure 2. X-ray diffraction (XRD) patterns of ruthenic acid nanosheet/Au films prepared by electrophoretic deposition of nanosheet colloids in a) acetonitrile and b) *N,N*-dimethylformamide. Peaks marked with asterisk are due to the Au substrate. The XRD patterns for c) tetrabutylammonium-ruthenic acid intercalation compound and d) layered ruthenic acid.

Figure 3. Surface scanning electron micrographs of ruthenic acid nanosheet/Au films prepared by electrophoretic deposition of nanosheet colloids in a) acetonitrile and b) *N,N*-dimethylformamide. EPD condition;  $E_{EPD}=5$  V,  $d_{EPD}=10$  mm,  $t_{EPD}=10$  min.

Figure 4. Steady-state cyclic voltammograms of ruthenic acid nanosheet/Au films

prepared by electrophoretic deposition of nanosheet colloids in a) acetonitrile and b) *N,N*-dimethylformamide, and the Au substrate at  $2 \text{ mV s}^{-1}$  in  $0.5 \text{ M H}_2\text{SO}_4$  ( $25^\circ\text{C}$ ). EPD condition;  $E_{\text{EPD}}=5 \text{ V}$ ,  $d_{\text{EPD}}=10 \text{ mm}$ ,  $t_{\text{EPD}}=10 \text{ min}$ .

Figure 5. Steady-state cyclic voltammograms of ruthenic acid nanosheet/Au films prepared by electrophoretic deposition of nanosheet colloids in *N,N*-dimethylformamide at  $2 \text{ mV s}^{-1}$  in  $0.5 \text{ M H}_2\text{SO}_4$  ( $25^\circ\text{C}$ ). EPD condition;  $E_{\text{EPD}}=5 \text{ V}$ ,  $d_{\text{EPD}}=10 \text{ mm}$ ,  $t_{\text{EPD}}=2-60 \text{ min}$ .

Figure 6. Specific capacitance of ruthenic acid nanosheet/Au films prepared by electrophoretic deposition of nanosheet colloids in *N,N*-dimethylformamide at 2-200  $\text{mV s}^{-1}$  in  $0.5 \text{ M H}_2\text{SO}_4$  ( $25^\circ\text{C}$ ). EPD conditions; electric field= $5 \text{ V cm}^{-1}$ , time=2-60 min.

Figure 7. Every 1,000th voltammogram from cycle no. 1,000 (dotted line) to 10,000 of ruthenic acid nanosheet/Au films prepared by electrophoretic deposition of nanosheet colloids in *N,N*-dimethylformamide at  $50 \text{ mV s}^{-1}$  in  $0.5 \text{ M H}_2\text{SO}_4$  ( $25^\circ\text{C}$ ). EPD

condition;  $E_{\text{EPD}}=5$  V,  $d_{\text{EPD}}=10$  mm,  $t_{\text{EPD}}=10$  min.

Figure 8. (a) Photographs of transparent HRONs/ITO-coated glass electrodes prepared by electrophoretic deposition of nanosheet colloids. EPD conditions;  $E_{\text{EPD}}=10$  V,  $d_{\text{EPD}}=20$  mm,  $t_{\text{EPD}}=15-120$  s. (b) A photograph of a flexible HRONs/ITO-coated PET electrode prepared by electrophoretic deposition of nanosheet colloids. EPD condition;  $E_{\text{EPD}}=5$  V,  $d_{\text{EPD}}=10$  mm,  $t_{\text{EPD}}=30$  min. (c) A side-view SEM image of a transparent HRONs/ITO-coated glass electrode prepared by electrophoretic deposition of nanosheet colloids. EPD condition;  $E_{\text{EPD}}=5$  V,  $d_{\text{EPD}}=10$  mm,  $t_{\text{EPD}}=2$  min x 15 times.

Figure 9. UV-vis of (a) bare ITO-coated glass electrode and HRONs/ITO-coated glass electrodes prepared under EPD conditions of  $E_{\text{EPD}}=10$  V,  $d_{\text{EPD}}=20$  mm and (b) 15, (c) 30, (d) 60, (e) 90, (f) 120 s.

Figure 10. (a) Cyclic voltammograms of ITO-coated glass/HRONs | Nafion117 | HRONs/ITO-coated glass transparent supercapacitor. EPD conditions;  $E_{\text{EPD}}=10$  V,  $d_{\text{EPD}}=$

20 mm,  $t_{\text{EPD}}=30$  s. (b) Capacitance of transparent supercapacitor as a function of  $t_{\text{EPD}}$ .

Figure 11. Constant current charge/discharge curves of ITO-coated glass/HROns | Nafion117 | HROns/ITO-coated glass transparent supercapacitor at (a) 3.2, (b) 32, and (c)  $320 \mu\text{A cm}^{-2}$ . EPD conditions;  $E_{\text{EPD}}=10$  V,  $d_{\text{EPD}}=20$  mm,  $t_{\text{EPD}}=30$  s.

Figure 12. Every 100th voltammogram from cycle no. 100 (dotted line) to 1,000 of ITO-coated glass/HROns | Nafion117 | HROns/ITO-coated glass transparent supercapacitor at  $50 \text{ mV s}^{-1}$ . EPD conditions;  $E_{\text{EPD}}=10$  V,  $d_{\text{EPD}}=20$  mm,  $t_{\text{EPD}}=30$  s.

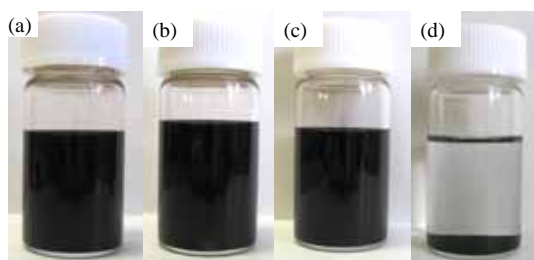


Figure 1

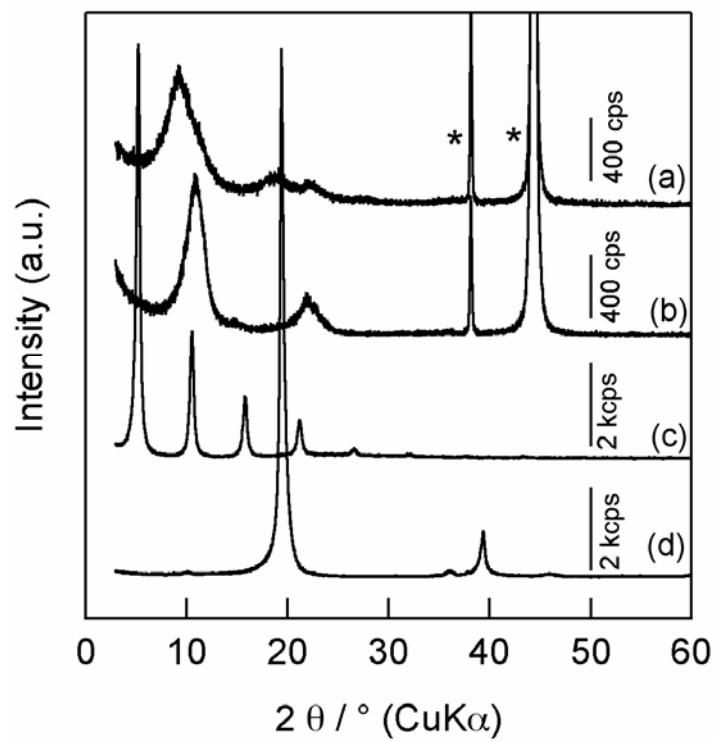


Figure 2

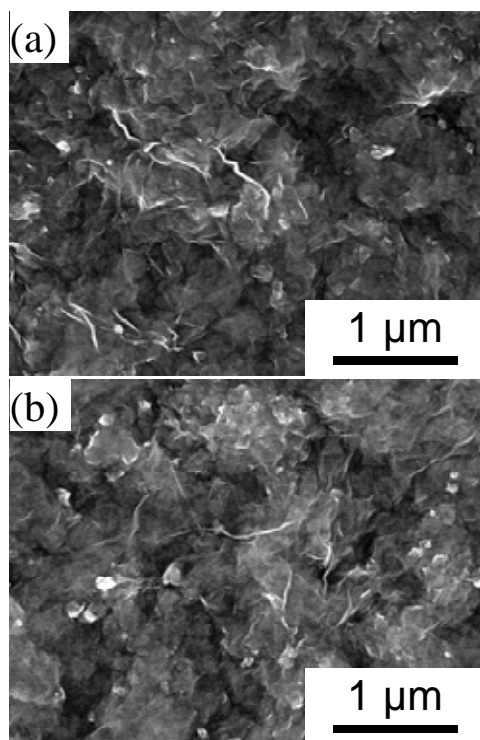


Figure 3

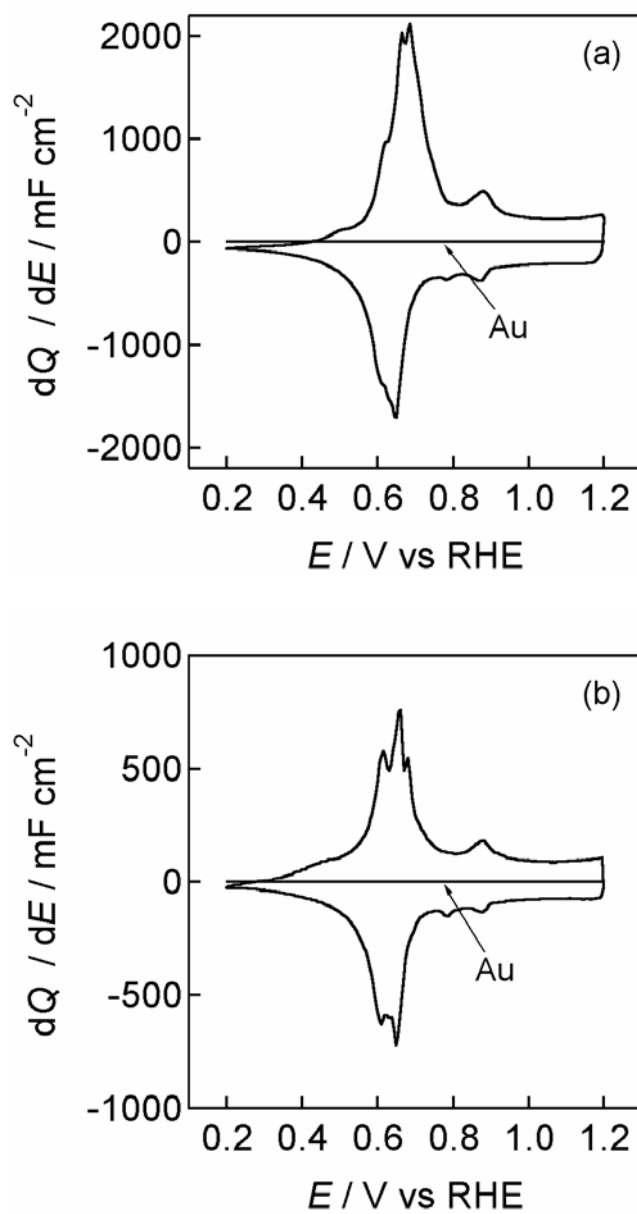


Figure 4

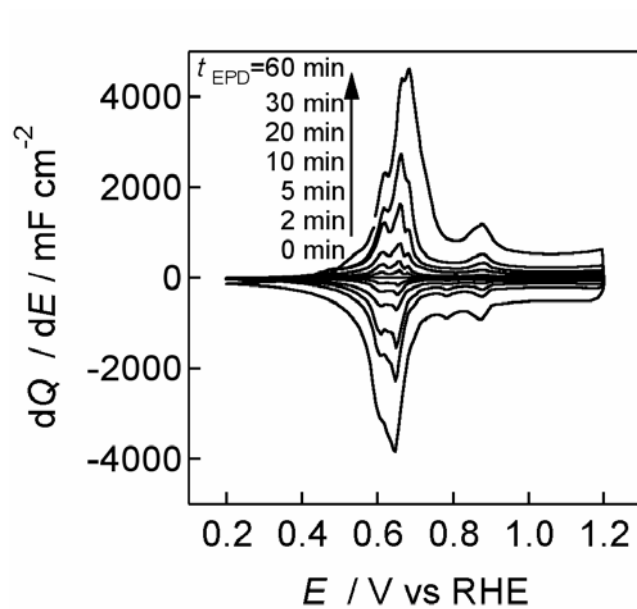


Figure 5

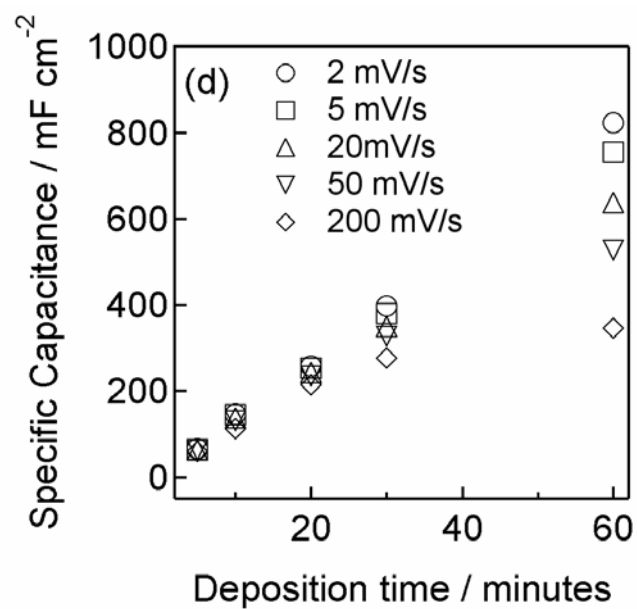


Figure 6

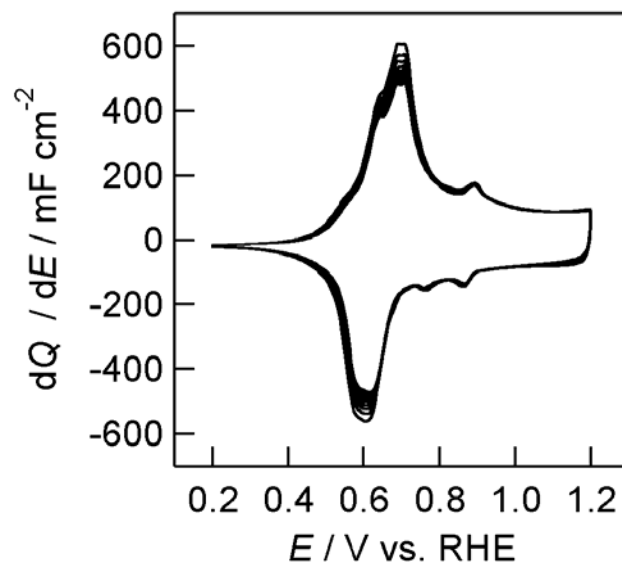


Figure 7

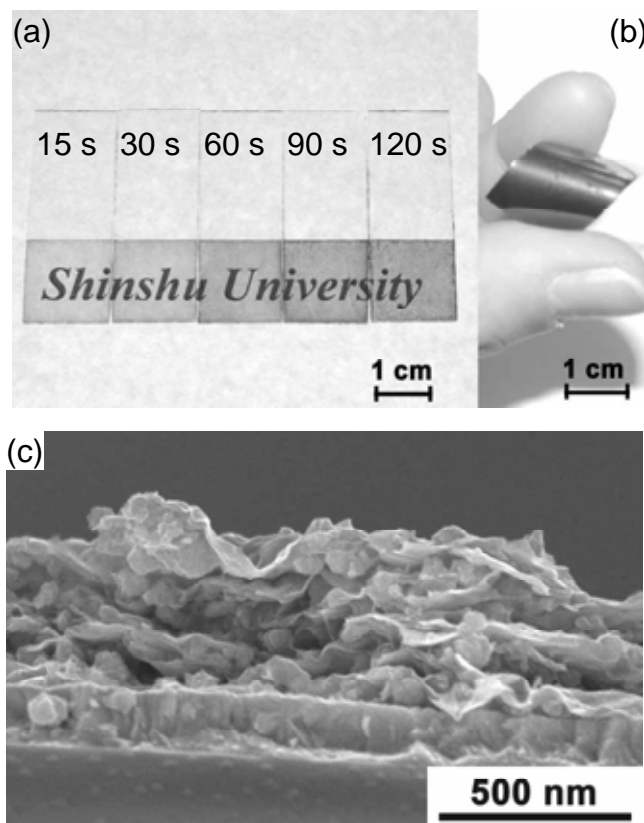


Figure 8

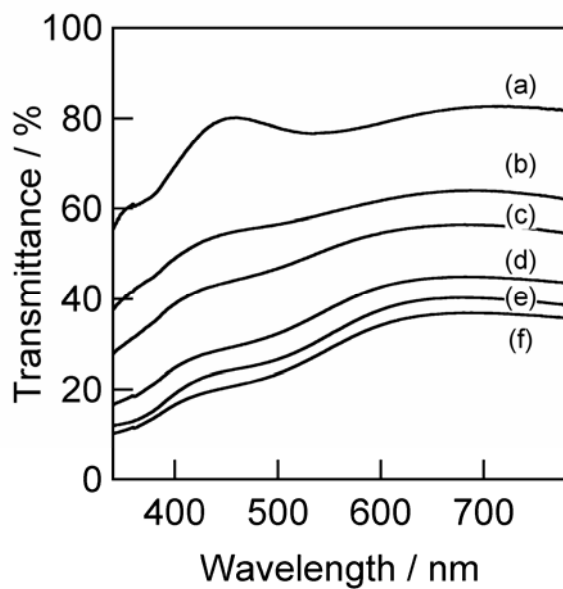


Figure 9

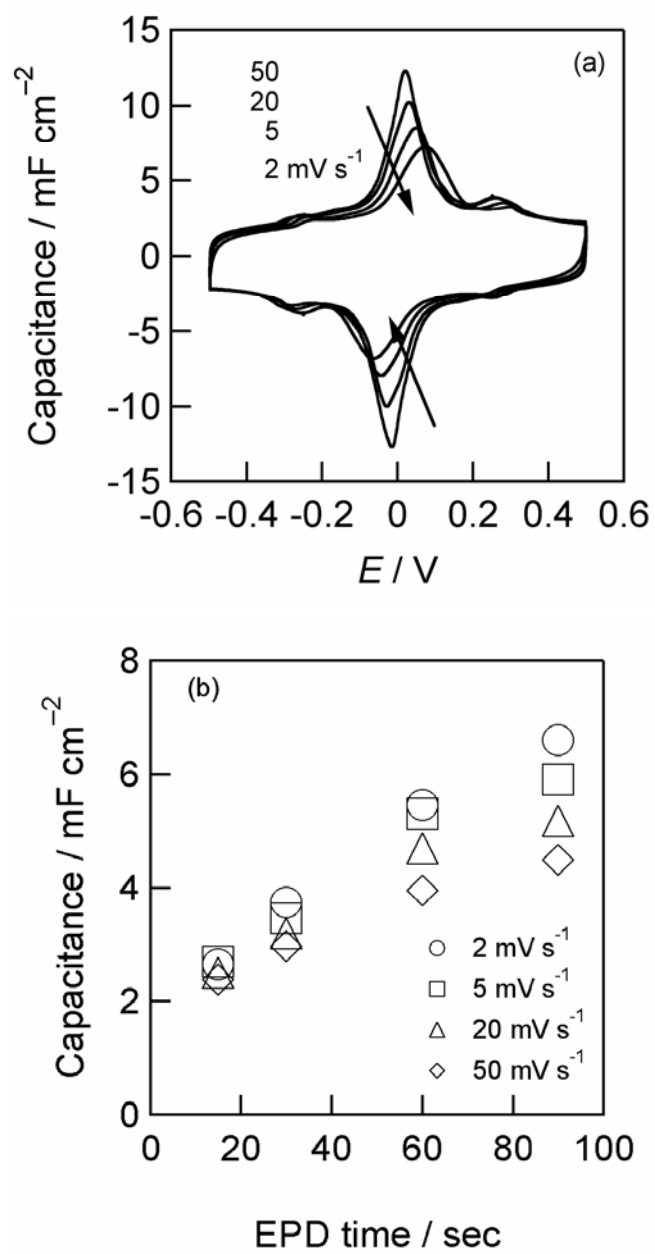


Figure 10

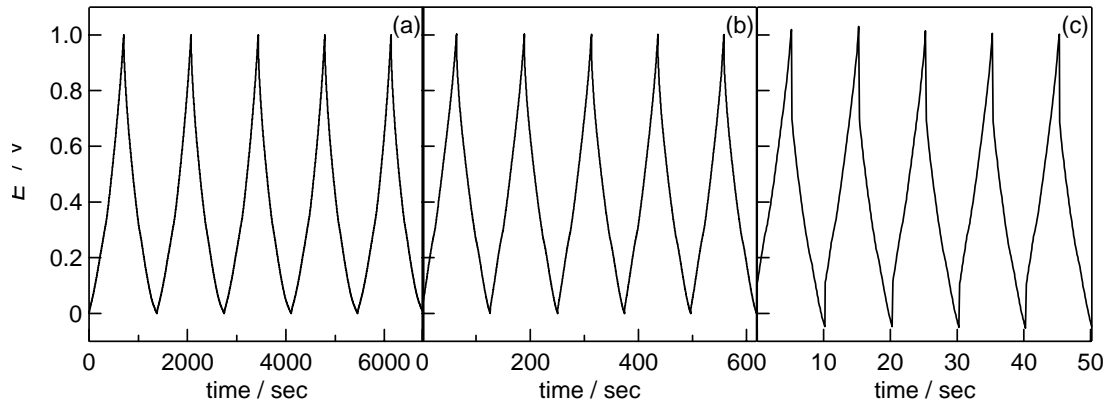


Figure 11

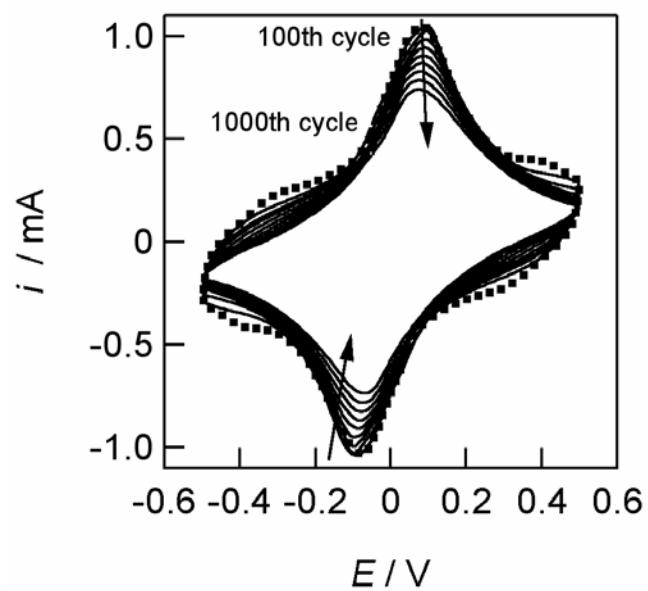


Figure 12